59th ILMENAU SCIENTIFIC COLLOQUIUM
Technische Universität Ilmenau, 11 – 15 September 2017
URN: urn:nbn:de:gbv:ilm1-2017iwk-068:4

INVESTIGATIONS ON MOTION DEVIATIONS OF AN EMFC BALANCE

Norbert Rogge[1], Jan Schleichert[1], Christian Rothleitner[2]

[1]Process Measurement Technology Group, TU Ilmenau, Germany
[2]Physikalisch-Technische Bundesanstalt (PTB) Division of Mechanics and Acoustics, Bundesallee 100, 38116 Braunschweig, Germany

ABSTRACT

This paper will present experiments to identify the angular misalignment and displacement of the coil movement of a commercial electromagnetic force compensated balance (EMFC) relative to the ideal trajectory. For this purpose the mechanical stability of measurement set-up and the environmental characteristics have to be taken into account. Considering the mass distribution of the moved coil carrier, that is not necessarily symmetric relative to the motion path of the coil carrier, the spring constants regarding torques applied to the coil carrier are important to evaluate the utilized balance. The investigations are performed with different excitation frequencies to evaluate the influence of the resonance behavior of the balance mechanics and the limitations it causes for the usability of the balance.
The measured deviations of the balance, planned to be used in the Planck-Balance set-up, depending on position and velocity of the coil will be shown and the effect of the observed deviations on the measurement uncertainty of the mass dissemination will be discussed.

Index Terms - electromagnetic force compensated balance, mechanical resonance, system identification

1. INTRODUCTION

The future redefinition of the kilogram will fix a value for the Planck constant and provide the mass by the measurement of time, length and electrical quantities [1]. Within the VIP+ project “Planck-Waage” (English: Planck-Balance) a device will be set up to disseminate this new definition of the mass not only for mass pieces of one kilogram, but also for smaller and arbitrary weights. The set-up will utilize a commercial EMFC balance notably for guiding the linear motion of the test coils that is necessary for the determination of the geometrical factor of the actuator. Assuming that the geometrical factor *Bl* of the actuator is the same for a voltage induced due a known velocity and a force generated by a measured current, both experiments can be utilized to cancel out the geometrical factor itself [2]. In order to insure the validity of this assumption, the motion has to be aligned to the force direction and should not possess rotations at the point of force measurement [3]. To reduce errors caused by deviations from a linear motion, these deviations have to be as small as possible and well known.
The use of a commercial standard weighing cell in a watt balance set-up is advantageous in terms of cost and development time. However, the characteristics of the motion of the balance which will be utilized have to be identified. In upcoming experiments an additional coil should be attached to the load carrier of the EMFC balance. In this configuration the motion and the force generation of the voice coil actuator is independent of the properties of the transmission lever system. Thus, the EMFC balance is merely used as mechanical guide system, but the actuator of the system can be used to apply additional forces for test purposes.

2. EXPERIMENTAL SET-UP

The investigated balance is a commercial EMFC balance with a measurement range of up to 200 g and a resolution of 0.1 mg. For internal self-calibration the balance is provided with two calibrated 100 g mass standards, which can be applied on special holders (see figure 1) that are attached to the load carrier (see figure 2). During normal operation of the EMFC balance these mass standards are used for recalibration of the device, but are not necessary in the Planck-Balance set-up. In this work they are utilized to modify the amount and distribution of moved mass on the load carrier. When placed on these holders, the centers of gravity of the mass pieces have a distance of 50 mm along z-axis (see figure 2) relative to the plane of symmetry of the balance.

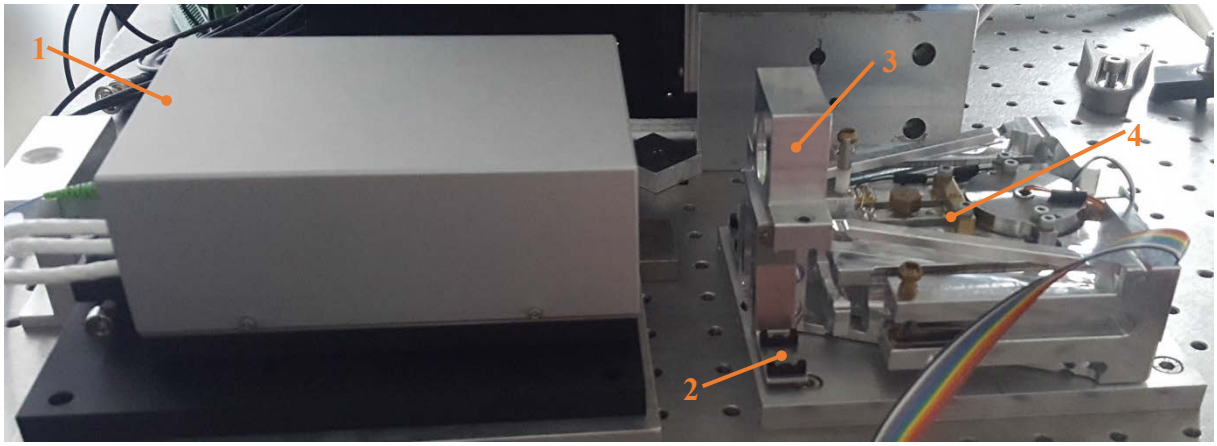

Figure 1: Utilized measurement set-up: 1 – Interferometer, 2 – holder for mass piece, 3 – mirror, 4 – EMFC balance.

The signal of the position sensor is measured by a digital signal processing system, on which the control algorithm is implemented. The position sensor consists of a vent at the end of the transmission lever, a LED and a differential photo diode. The light of the LED passes the vent and generates a photo current in each of the halves of the differential photo diode. The photo currents are utilized to produce a voltage signal, which yields a value of zero when both halves receive the same amount of light. The signal of the position sensor is used to calculate the controller output voltage that is necessary to hold zero position and an amplifier circuit provides the current of the balances voice coil actuator proportional to the controller output voltage. In contrast to the signal of the interferometer, the signal of the internal position sensor of the balance provides information of an absolute deflection of the lever and remains its zero reference position even after temporary power shutdown. Therefore, it is also used to provide a reference point for the measurement with the interferometer.
The motion of the load carrier is observed with an interferometer with three parallel beams. As each beam is part of an independent Michelson interferometer, the displacement of three points on the surface of the mirror, which is placed on the load carrier, can be measured. Given that the distance between the laser spots is known and the spots represent the corners of a rectangular triangle, two tilt angles can be calculated in addition to the displacement that is measured directly. In order to characterize all rotational motion deviations of the load carrier, the interferometer is used in two configurations as depicted in figure 2. In the first configuration, the beams are aligned along the y-axis and thus the displacement in the vertical direction and the rotation around the z-axis and x-axis can be observed. In the second configuration the beams are aligned along the x-axis, to measure the horizontal parasitic displacement and the rotation around the y-axis and z-axis. As the rotation around the z-axis

is observed in both configurations, it will be used in section 3.1 to evaluate if the results are consistent.

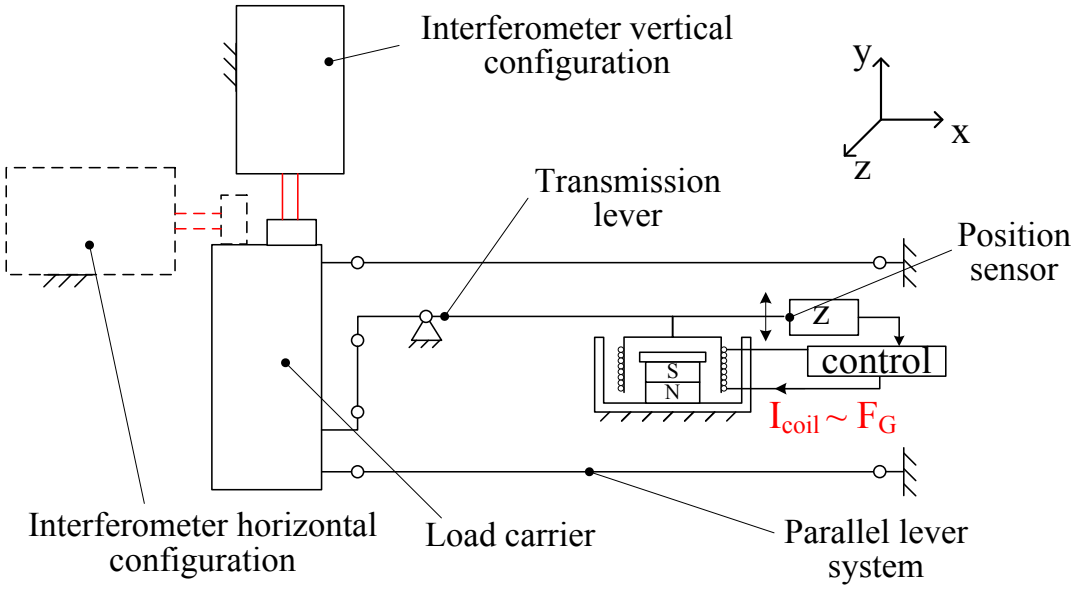

Figure 2: Schematic view on the measurement set-up.

The limited mechanical stability of the mounting of the interferometer causes drift effects within the signals of displacement and tilt. The investigations in this work are focused on systematical tilt and displacement errors that are caused by inevitable deviations from an ideal parallel lever system with equally distributed elasticity. Since the drift errors are of minor concern in this work, they are corrected by measuring displacement and tilt relative to the zero position of the controlled balance. For the planned Planck-Balance experiments, the drift effects must be reduced by utilizing a mounting frame with higher mechanical stability.

3. MEASUREMENT RESULTS

3.1 Static displacement

Due to geometric considerations, it is expected that the desired vertical movement s_y of the load carrier also causes a parasitic horizontal motion s_x:

$$s_x = \frac{s_y^2}{2L_l}, \tag{1}$$

where L_l is the length of the parallel levers. In order to compare this expected to the real behavior of the balance, the set point of the position controller was changed stepwise within the mechanical limits of the lever motion. In the vertical configuration, the measurement data of the interferometer and the position sensor is used to identify the coefficients of a polynomial that is a best fit to the relation between the measured position voltage and the vertical displacement measurement in meters. The obtained coefficients are later used to calculate the vertical displacement of the load carrier in order to provide also the vertical displacement in the horizontal configuration in which only the horizontal displacement is directly measured.

Figure 3 shows the horizontal parasitic displacement as a function of the vertical displacement that is calculated from the position sensor signal. The shown graph is obtained by removing the trend ($2.2 \cdot 10^{-3}$ m/m) of the measured displacement signal, which represents the

misalignment between the motion axis of the load carrier and the ideal axis that is orthogonal to the interferometer beams. Since this misalignment is of minor interest for the investigation on the parasitic movement, it was removed from the graph. The expected behavior described by equation (1) shows only deviations smaller than 1 nm and therefore the parasitic horizontal displacement can be modelled with sufficient accuracy by these simple geometrical considerations. Furthermore, it can be observed that the minimum of the graph is located almost exactly in the middle of the possible motion range. Actually, the best fit between the measured and the calculated displacement can be achieved for an offset of 2.2 nm within the y-axis. This is beneficial for the calibration of the geometrical factor of the actuator, since the deviation of the direction of motion from the direction of an applied force is smallest at this point.

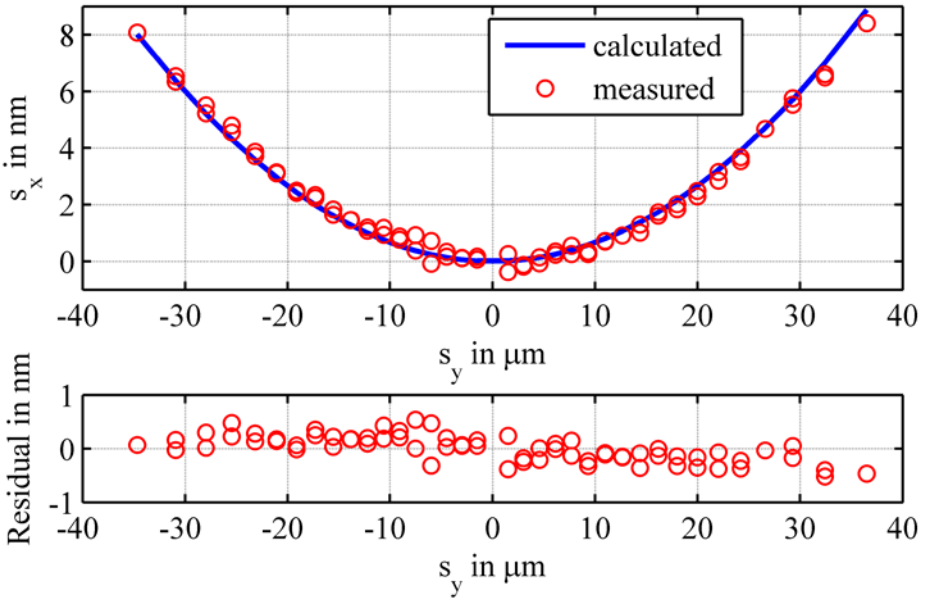

Figure 3: Horizontal displacement of the load carrier along the vertical motion range.

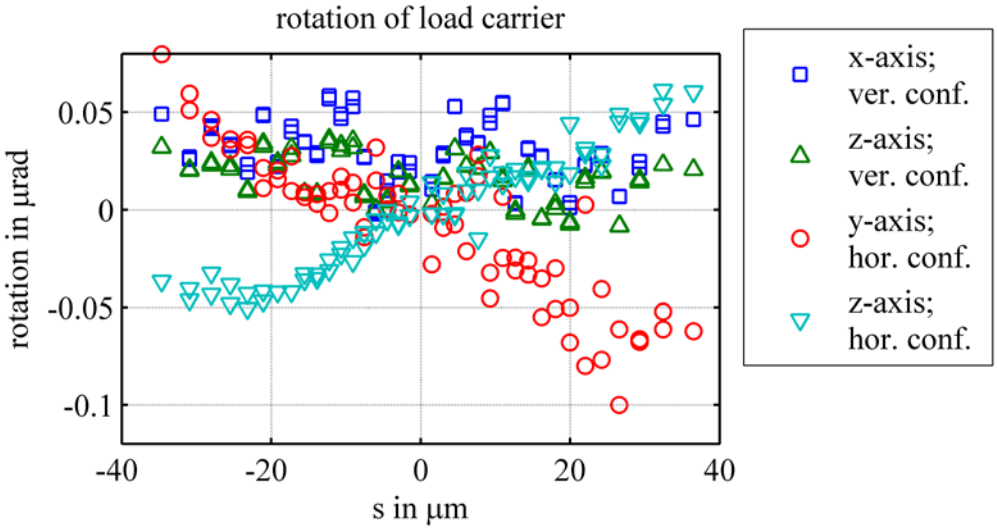

Figure 4: Measured rotation of load carrier for both configurations. (ver. conf. = vertical configuration, hor. conf. = horizontal configuration)

Another type of parasitic motion that can occur is the rotation of the load carrier. The rotations around all three axes are calculated for each step for the measurements in vertical

and horizontal configuration from the additional displacements of the two other beams. Similar to the measurement of the deflection, the rotation is measured relative to the zero position and is presented in figure 4. The rotations measured in the vertical configuration show no significant effect depending on the displacement of the load carrier. In contrast the rotations observed in the horizontal configuration seem to show a small but significant change along the vertical movement. However, the observed values correlate to a displacement difference of 22 nm measured by one of three beams. As the utilized mirror is specified with a flatness of 63 nm, the change can be caused by the greater movement of the laser spots on the mirror surface in horizontal configuration. The utilized laser spots possess a diameter of 1 mm and are placed close to the edge of the mirror and are not able to reduce errors caused by the planarity deviations of the mirror. This effect also explains the differences between the observations for the rotation around the z-axis within the comparison of the two configurations. Nonetheless, a rotational movement of the load carrier greater than ±100 nrad is unlikely regarding to the observed behavior.

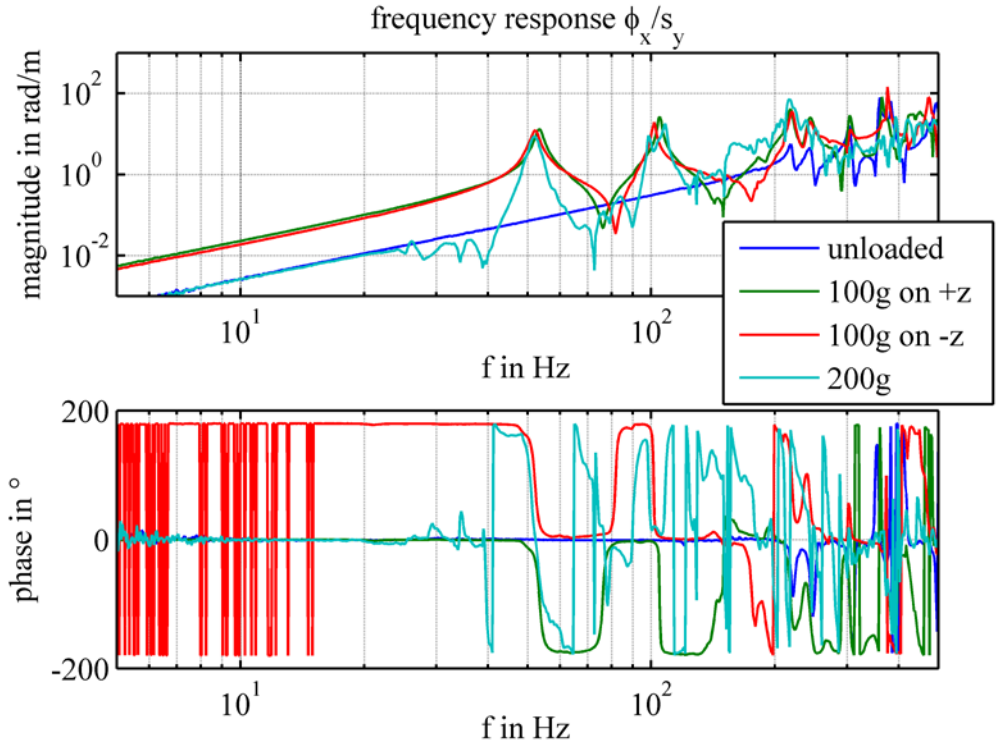

Figure 5: Frequency response of the rotation ϕ_x around the x-axis relative to the vertical displacement s_y.

3.2 Dynamic behavior

Hence the determination of the geometrical factor of the actuator is planned to be utilizing a sinusoidal motion of the load carrier, the motion deviations have to be investigated at different frequencies of excitation. In the performed experiments a chirp signal was added to the set point value of the position controller to excite the mechanical system at different frequencies. The signal frequency raises from 1 Hz to 30 Hz, but due to the nonlinear relation between position voltage signal and displacement, the signals of the interferometer also exhibits amplitudes at higher frequencies. The experiments were performed without additional mass on the load carrier and a symmetrical distributed mass of 200 g. The influence of an unsymmetrical distributed moved mass has been investigated by putting only one 100 g mass either on the holder in positive direction of the z-axis or on the holder in negative direction.

All measured rotation signals are set into relation to the desired displacement along the y-axis to focus on rotational motions that are correlated with the harmonic excitation of the load carrier.
The Bode plot of the rotation around the x-axis that is stimulated by the motion along the y-axis (figure 5) shows a linearly increasing magnitude and constant phase relation with increasing frequency for all loads. In case of a 200 g load on the carrier, significant deviations from this behavior occur at frequencies of 20 Hz and above. In contrast to other observed effects, these deviations are reduced, when the amplitude of excitation is decreased (see figure 6). Therefore, they can supposedly be considered as nonlinear effects.

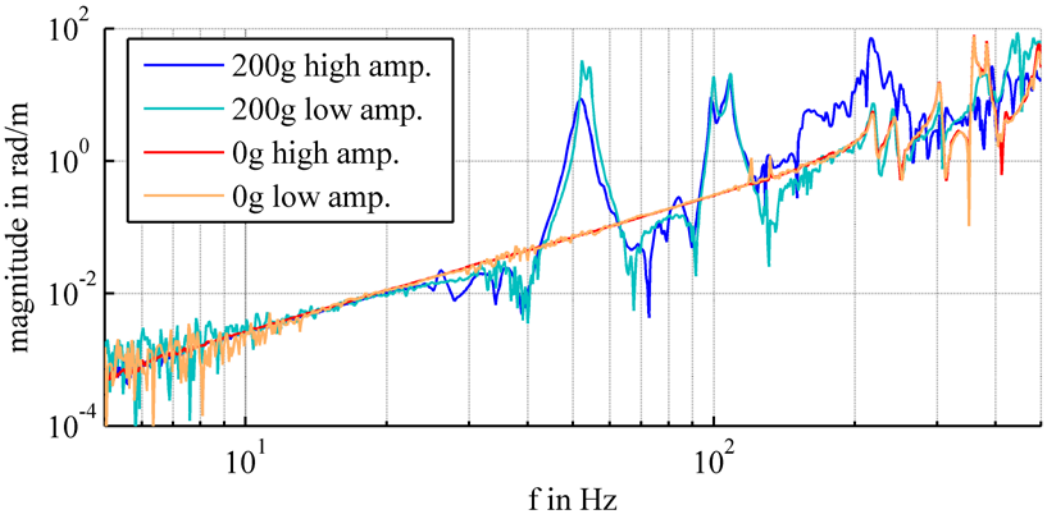

Figure 6: Magnitude of the frequency response of the rotation ϕ_x around the x-axis for different amplitudes of excitation. (amp. = amplitude)

Considering smaller loads than 200 g, the deviations from a linear increase in the lowest frequency range coincide with a mechanical resonance at approximately 53 Hz. Since the phase shift between rotation and vertical displacement changes in the range of the resonance frequency, this frequency range should be avoided for a determination of the geometrical factor. The rotational oscillation in the lower frequency range is less problematic due to the constant phase shift of zero or ±180 degrees (the phase shift by ±180 degree is caused by phase wrapping). In the course of a sinusoidal motion of the load carrier these values of phase shifts imply that the rotation is also zero when the displacement is in zero position. For this position the absence of a rotation of the load carrier is beneficial in order to match the direction of the force within the weighing experiment and the direction of movement in the experiment to obtain the geometrical factor of the actuator.
Nonetheless, the rotation angles are not only important for retaining the adjustment of direction for the force and velocity experiments, but also does a change of the rotational angle cause a contribution to the error of the determined geometrical factor itself [4]. The angular velocity ω_i during a sinusoidal motion can be obtained from the measured angle ϕ_i by differentiation:

$$\omega_i = \frac{\partial \phi_i}{\partial t} = 2\pi f \hat{\phi} \sin\left(2\pi f t + \theta_0 + \frac{\pi}{2}\right), \quad \text{with: } \phi_i = \hat{\phi} \sin(2\pi f t + \theta_0)\,. \tag{2}$$

Since the measured amplitude $\hat{\phi}$ increases linearly with higher frequencies, the amplitude of angular velocity increases quadratically. At zero position of the displacement the absolute

value of the angular velocity reaches its peak value due to the constant phase shift of 90 degrees in the previously mentioned range of the linear magnitude increase. According to Li et al [4] the error contribution of the angular velocity is depending on the product $\omega_i\phi_i$ and is therefore also small for small absolute rotational angles. However, the mentioned relation applies to a coil that is placed symmetric to the axis of rotation. Given a distance d_c between the center of the coil and the rotational axis, the coil performs a translational displacement of $s_T \approx d_c \cdot \phi_i$ with the velocity $v_T \approx d_c \cdot \omega_i$ for small angles. As this error is also expected to occur in the range of the linear magnitude increase, the frequency of a sinusoidal motion and the coil distance should be kept small to reduce these errors.

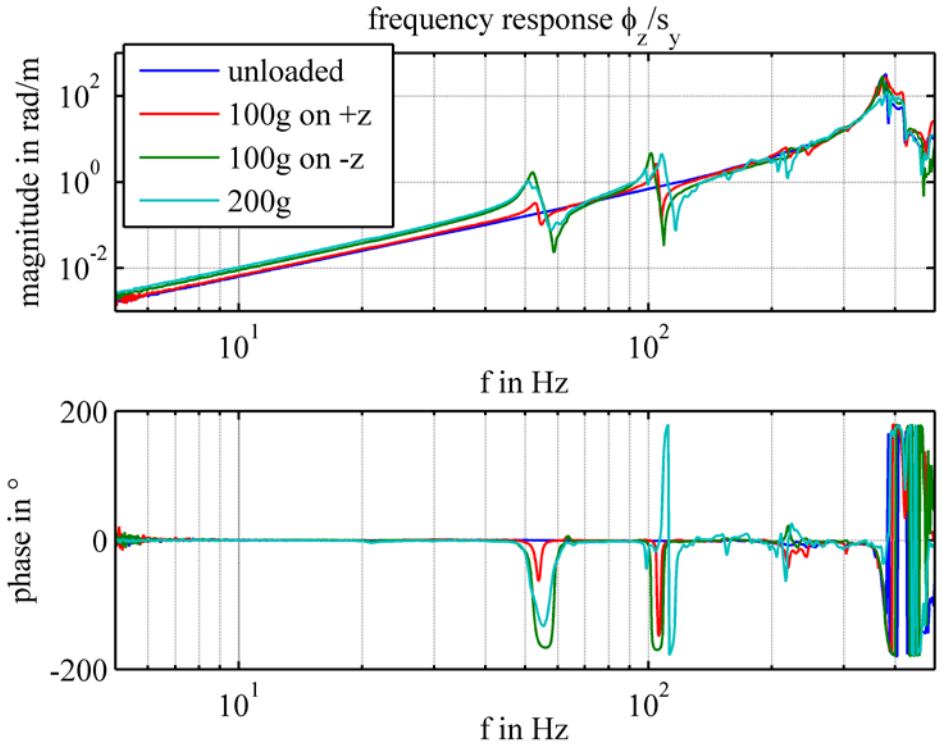

Figure 7: Frequency response of the rotation ϕ_z around the z-axis relative to the vertical displacement s_y.

In addition to a reduction of the moved mass, the distribution of mass should preferably be symmetric to the balance's lever. Otherwise the magnitude of rotational motion around the x-axis increases by a factor 10, while the phase shift shows oscillations in the opposite direction in case of a higher load on the negative z-axis (figure 5).
The effects described for angular motion around x-axis appear similarly for the motion around the z-axis despite the fact, that greater differences are only expected in case of an asymmetric mass distribution along the x-axis. Given that this distribution can be hardly influenced in the presented set-up, the results for the different loads are more alike regarding this rotational axis (figure 7).
Regarding the rotation around the y-axis (figure 8), the dynamic behavior cannot be related to the vertical displacement directly as this rotation is only observed in the horizontal configuration of the presented set-up. Therefore, the transfer behavior was calculated by:

$$G_{\phi,y}(s) = \frac{\phi_y}{s_y} = \frac{\tilde{G}_{\phi,y}(s)}{G_{y,c}(s)} \tag{3}$$
$$\text{with: } \tilde{G}_{\phi,y}(s) = \frac{\phi_y}{s_c} \text{ and } G_{y,c}(s) = \frac{s_y}{s_c}$$

where the position signal s_c can be obtained in both configurations and is utilized by determining $\tilde{G}_{\phi,y}(s)$ in horizontal configuration and $G_{y,c}(s)$ in vertical configuration. Within the lower frequency range, the magnitudes observed for this type of rotation is by a factor 10 to 100 smaller than the ones observed for the other rotational axis. Furthermore it causes no motion orthogonal to the magnetic field of the actuator and could only yield errors due to deviations from its azimuthal symmetry [4]. Hence, the errors caused by rotational motion around y-axis can be neglected, if the requirements regarding excitation frequency and alignment are fulfilled.

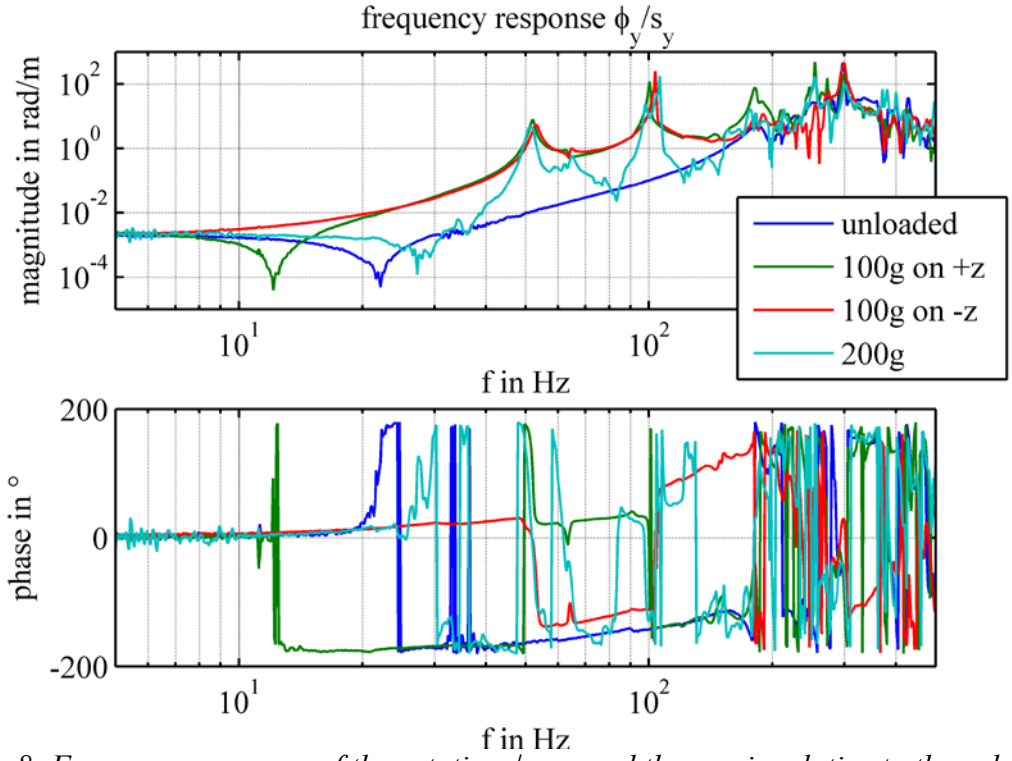

Figure 8: Frequency response of the rotation ϕ_y around the y-axis relative to the calculated vertical displacement s_y.

As shown in figure 3, the horizontal translational motion possesses a nonlinear dependency on the vertical motion. Considering the utilized amplitude of the vertical motion, this effect should yield a magnitude of $2 \cdot 10^{-4}$ m/m. However, this contribution to the horizontal motion is negligible since the observed magnitude is significantly greater (figure 9). In contrast, the linear relation between horizontal and vertical motion that is generated by the misalignment of the beam axes fits to the observed magnitude at frequencies lower than 20 Hz. Furthermore, the mirror is not well aligned with the center of rotation around the z-axis, yielding an additional horizontal motion. Based on geometrical considerations and the results depicted in figure 7, a magnitude of approximately $2 \cdot 10^{-3}$ m/m at a frequency of 20 Hz is expected. Given that this horizontal motion effect occurs in opposite direction to the effect caused by the misalignment, the measured magnitude decreases with increasing frequency before it rises to

its first resonance peak. Since the observed dynamic horizontal displacement increases at frequencies of up to 30 Hz, the frequency limits derived from the rotational motion also keep the horizontal motion minimal.

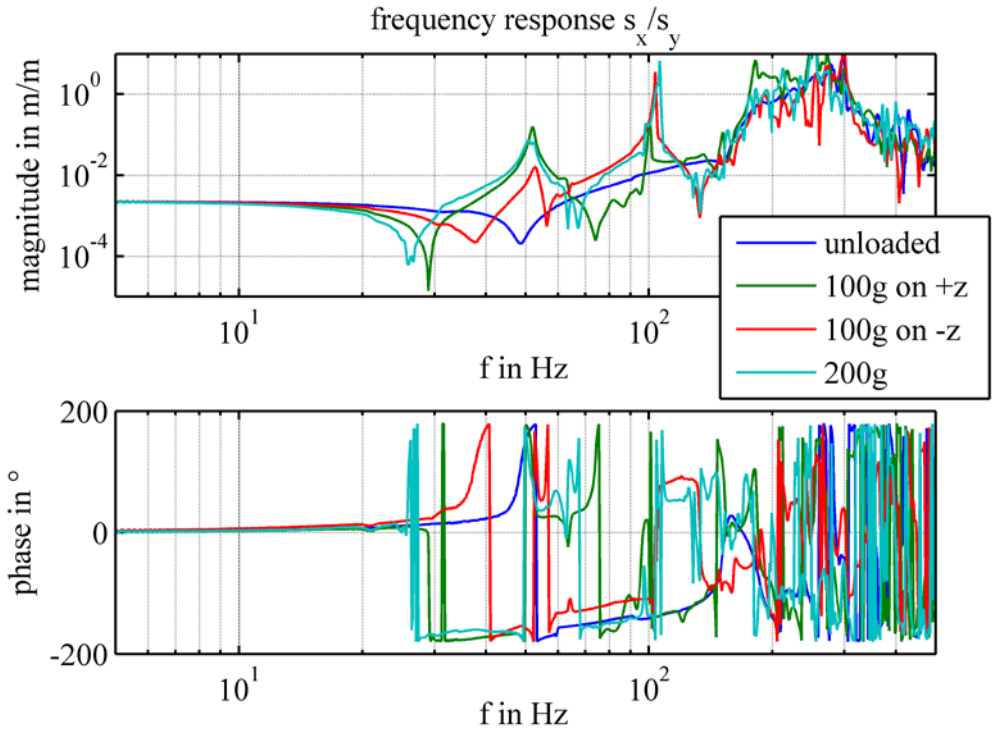

Figure 9: Frequency response of the horizontal motion s_x relative to the calculated vertical displacement s_y.

4. CONCLUSION

The presented results show, that a commercial EMFC balance possesses an almost ideal characteristic regarding to the static motion deviations. The horizontal displacement that is inevitably due to the use of a parallel lever system meets precisely the expected values. Within the static experiments, there was no significant angular deviation greater than ±100 nrad and therefore the direction of motion with low speed is well adjusted to the direction of force in the weighing experiment. Dynamic rotation occurs with an increasing magnitude and constant phase shift for the most relevant rotations around the x-axis and z-axis in a frequency range of up to 30 Hz. In this frequency range the only deviations from the behavior of an ideally stiff load carrier are rotational oscillations with a constant or linear increasing magnitude and constant phase shift. At higher frequencies resonance phenomena occur along with a disadvantageous phase shift that must be avoided in the planned experiments. To achieve low magnitudes of motion deviations, the mass attached to the load carrier should be as low as possible and symmetrically distributed. Horizontal motions along the x-axis are observed with a magnitude of $2.2 \cdot 10^{-3}$ m/m in the lower frequency range, but are consistent with the determined misalignment of the measurement axis. Therefore, the distance between the axis of rotation and the actuator coil should possibly be kept low.

5. ACKNOWLEDGEMENT

The research of this project is funded via the programme “Validierung des technologischen und gesellschaftlichen Innovationspotenzials – VIP+” of the German Federal Ministry of Education and Research (BMBF), and is managed by the VDI/VDE Innovation + Technik GmbH.

REFERENCES

[1] CCM “Report of the 14th Meeting of the CCM”, BIPM, Sèvres, 2013.
[2] B. P. Kibble, “A measurement of the gyromagnetic ratio of the proton by the strong field method”, Atomic Masses and Fundamental Constants 5, ed J H Sanders and A H Wapstra, New York, pp 545–51, 1976.
[3] M. Stock, “Watt balance experiments for the determination of the Planck constant and the redefinition of the kilogram”, Metrologia 50 R1-16, 2016.
[4] S. Li, S. Schlamminger, D. Haddad, F. Seifert, L. Chao, J. R. Pratt, “Coil motion effects in watt balances: a theoretical check”, Metrologia 53 817, 2016.

CONTACTS

M.Sc. Norbert Rogge norbert.rogge@tu-ilmenau.de
Dr. Christian Rothleitner christian.rothleitner@ptb.de

